Characterizing Dust Contamination in Advanced Virgo

REU Final Report
Emily Duden
Mentor: Dr. Giacomo Ciani (Universita di Padova)
August 14th, 2020
Funded by NSF REU Program #1460803/#1950830 and University of Florida

Dust contamination, while extremely low in the cleanroom environment of Virgo, is a common source of light scattering in optical systems. Given the incredible sensitivity of current gravitational wave detectors, even the small amount of dust present can have a significant effect on measurements. It is therefore critical to identify the distribution of dust particles on optical elements to determine the noise introduced into measurements. After analyzing images taken in the squeezed vacuum (SQZ) subsystem, we propose a procedure for characterizing dust contamination in advanced Virgo and present estimates for dust levels in the SQZ subsystem.

1. Introduction

1.1. Advanced Virgo

Advanced Virgo is a gravitational wave detector located near Pisa, Italy and hosted by the European Gravitational Wave Observatory (EGO). A laser interferometer with perpendicular 3 km arms (Fig. 1), it has been an integral part of gravitational physics since the first gravitational wave detection in 2015. In an interferometer, light of a fixed wavelength is sent down the two arms before recombining at the detector, where its phase is measured. Incoming gravitational waves distort spacetime, causing one arm to be longer than the other and changing the phase detected [1].

Within Advanced Virgo, the squeezed vacuum (SQZ) subsystem helps to reduce quantum noise. But as with any optical system, it is subject to light scattering, which leads to further noise in the detector. Here, we study how dust in the SQZ subsystem produces such scattering.

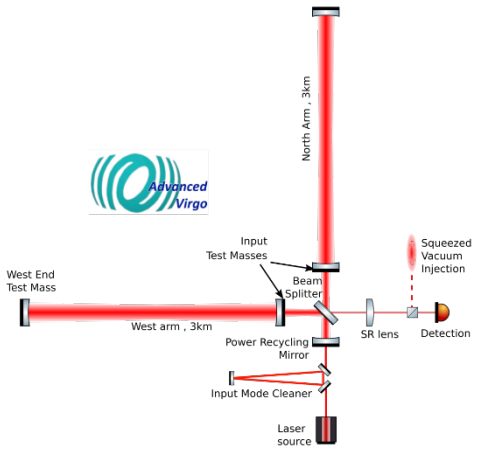

FIG 1: Optical layout of Advanced Virgo. In this paper, we study scattered light due to the SQZ subsystem, which is responsible for the squeezed vacuum injection.

1.2. Scattered Light

Scattered light is light which deviates from the expected (or nominal) path in an optical system. Two of the most common progenitors of scattered light are the residual surface roughness of optical elements and contamination from particulates. Our investigation focuses on the latter, which is described by Mie scattering theory. This light, the phase of which differs randomly from the nominal light, adds noise to the measured phase by recombining with the nominal light. Further, optical elements move slightly due to uncontrollable factors such as seismic activity, causing the phase change due to scattered light to be unstable. Since the detection of gravitational waves requires measurement of a phase difference on the order of 10^{-12} photon wavelengths, just a few stray photons with a random phase difference may be of great detriment to gravitational wave detection [2].

1.3. Mie Theory and the Particle Density Function

Mie scattering theory describes scattering due to particles with diameter on the order of incident photon wavelength or greater. It predicts the bidirectional scattering distribution function (BSDF), which describes how the light is scattered [2]. The BSDF relies on the particle density function $f(D)$, which describes the cleanliness of an optical surface and is given by

$$f(D) = -\frac{d}{dD} N_p(S,\ CL,\ D) \tag{1}$$

where N_p is the number of particles per 0.1 m^2 with diameter greater than or equal to D, the particle diameter in μm. IEST-STD-CC1246D defines N_p as

$$N_p(S, CL, D) = 10^{|S|[\log_{10}^2(CL) - \log_{10}^2(D)]}. \tag{2}$$

S, called the particle distribution slope, is the slope of a plot of N_p versus D on a log-log^2 scale. S depends on the cleanliness of the environment and process used to clean the surface. CL is the cleanliness level of the surface in μm, which corresponds by definition to the diameter of the particle whose density is 1/0.1 m^2 [3]. Note that due to the logarithmic nature of N_p, IEST-STD-CC1246D is only valid for $D \geq 1\ \mu m$.

Lower values of S correspond to cleaner surfaces, since cleaning tends to remove larger particles and leave smaller ones [2]. IEST-STD-CC1246D defines an S value of -0.926 for recently cleaned surfaces. However, this slope is an idealized case and has never been experimentally observed. For instance, Hamberg and Shon summarize experimental results from clean rooms throughout the aerospace industry, finding and average slope of -0.383 [4]. Other attempts [5, 6] have been made to more accurately model S, but it remains most appropriate to calculate S for each environment.

Dust scattering analyses will be carried out with FRED Optical Engineering Software, which relies on Mie theory and thus requires an input particle distribution. This particle distribution can be modelled or derived; FRED includes models IEST-STD-CC1246D, Gaussian distribution of particles by diameter, and uniform distribution of particles by diameter.

2. Witness Wafer Imaging Procedure

In order to characterize dust contamination, surfaces must be inspected, and all dust particles must be counted. To do this, several silicon "witness" wafers 2" and 3" in diameter were placed throughout the SQZ chamber in open boxes, clean faces exposed, with their box lids facing downward next to them in preparation for transportation. After 30 days, the samples were removed [7].

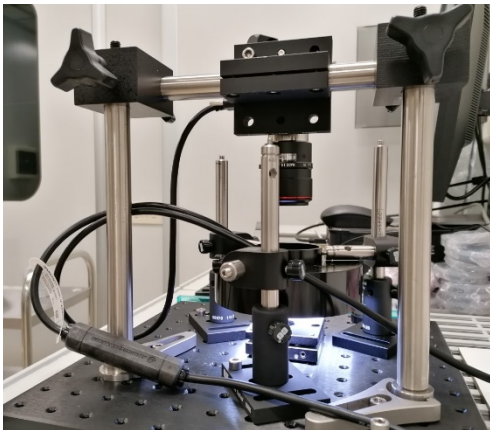

FIG 2: Wafer imaging setup. An illuminating LED ring is set 60 mm above the table, with the sample placed on a platform a few centimeters high.

The samples were then imaged using a 10 MP camera with 2/3" sensor and 35 mm focal length, alongside a high-resolution lens at working distance 110 mm (procedure outlined by Sorrentino [8]). Images were taken with an illuminating LED ring set ~40 mm and ~60 mm above the table (with the sample itself placed a few centimeters above the table), an exposure time of 56 ms, and numerical aperture (NA) values of 5.6, 8, and 16 (imaging setup shown in Fig. 2). The result of different imaging parameters is shown in Fig. 3. The best images were obtained with the LED height 60 mm and numerical aperture 5.6. It was deemed unnecessary to use a box over the imaging instruments to reduce scatter and glare, since the effects of the box were not immediately evident and its use likely generated some particle fallout on the samples.

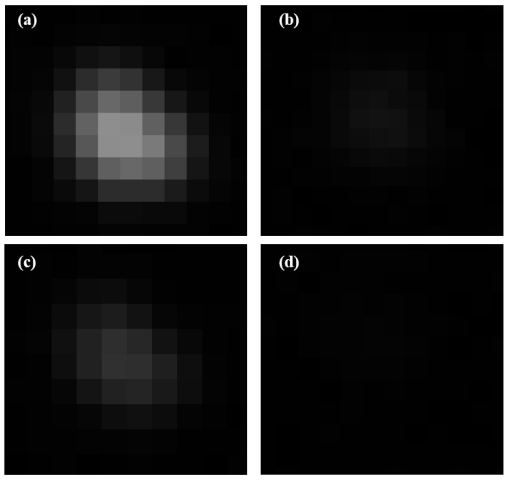

FIG 3: Particle after combining six nominally identical images with parameters **(a)** $NA = 8$ and LED height 56 mm, **(b)** $NA = 16$ and LED height 56 mm, **(c)** $NA = 8$ and LED height 45 mm, and **(d)** $NA = 16$ and LED height 45 mm.

Since the luminosity of pixels display slight random fluctuations, some background pixels may appear particle-like during image analysis. To prevent this, at minimum two nominally identical images must be taken and combined. However, background pixels become easier to disregard the more images are combined, so we suggest taking four nominally identical images for each region whenever possible.

3. Image Analysis

After obtaining high-quality images of the witness wafers, the images were imported as stacks into ImageJ and combined by assigning each pixel its minimum value in the stack. Next, the images were processed and the dust particles counted. ImageJ, Toupview, and MATLAB image processing software were used to count particles and their results were compared. MATLAB was selected, as it is significantly faster to use and all three software yielded nearly

identical results. Additionally, MATLAB can easily output other useful parameters, such as particle location.

Images were processed in MATLAB using an updated version of the code authored by Waller [9], described by the following steps:

Import image
Subtract background illumination
Convert image to grayscale
Convert grayscale image to binary
Remove particles above or below a chosen size from binary image
Print binary image
Outline, number, and label particles on binary image
Measure area of particles
Determine location of particles
Measure major and minor axes of ellipses drawn around particles
Output particle labels, areas, locations, and ellipse aspect ratios to csv file

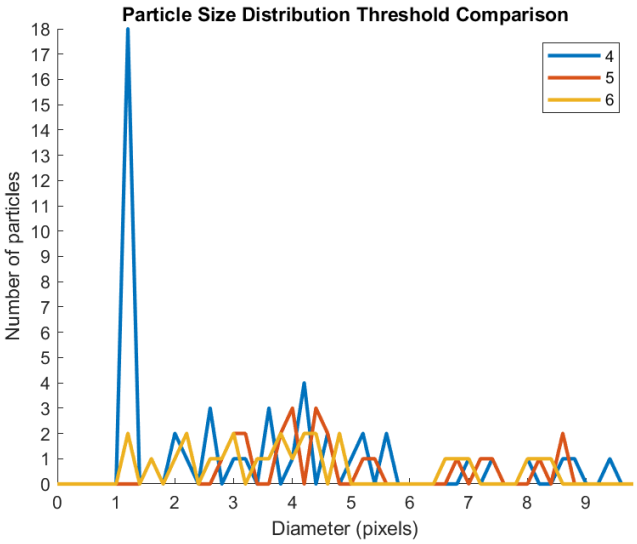

FIG 4: Particle distribution by diameter for thresholds set to luminosity 4, 5, and 6 (out of 256 levels). We include many background pixels in our particle count at threshold 4.

When converting the grayscale image to binary, one must input a threshold value. Pixels with luminosity below this value have luminosity set to 0, while pixels above or equal to the threshold have luminosity set to 1. Given the large effect this variable has on particle count and size, it is important to select a threshold that accurately distinguishes between particle and background. As mentioned above, combining multiple nominally identical images greatly reduces background and increases the range of threshold values that yield accurate results. Fig. 4 displays the effect of threshold on particle detection.

4. Results

We first analyzed cleanliness data from various cleanrooms in LIGO, reported in the LIGO Document Control Center (DCC) and logbook (LLO) [10, 11]. Plots of N_p versus particle diameter in μm were fit to Eq. 2 to determine cleanliness level CL and particle distribution slope

S. We then plotted the total number of particles per 0.1 m^2 versus slope (Fig. 5), with the intent to find a relationship between surface cleanliness and S. However, we discerned no clear pattern. Data were also compared based on location, date, and work done in their proximity. While surfaces imaged after cleaning procedures and before exposure to extensive activities were generally cleaner, we found no connection with S. It is worthwhile to note that while Eq. 2 suggests that plots of N_p on a log-log^2 scale should be linear, many distributions were clearly not linear. Even after removing these curved distributions from our analysis, we could find no meaningful relationship between surface cleanliness and S.

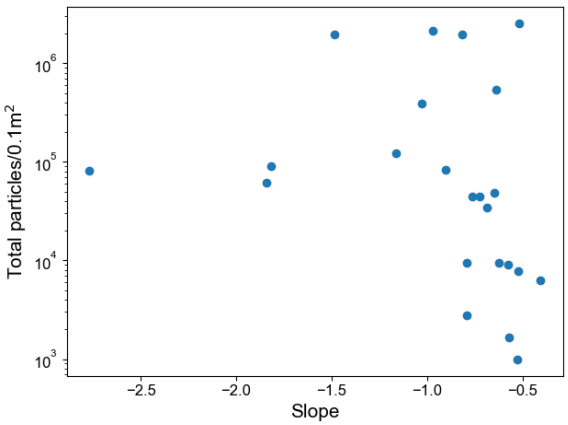

FIG 5: Total number of particles/0.1 m^2 versus particle distribution slope S for various locations in LIGO. No discernable pattern was found.

Next, we analyzed images taken around the SQZ subsystem using the procedure outlined above. Once particle counts were obtained, we calculated particle diameters in pixels by assuming perfect circularity. These diameters were converted into μm, and N_p was plotted on a log-log^2 scale and fit with Eq. 2. One such plot is shown in Fig. 6. The results of fits to images taken with numerical aperture 5.6 and LED height 60 mm are found in Fig. 7. All wafers were exposed for one month and placed horizontally unless otherwise noted in the table. These fit results are notably similar considering the samples' wide variety of placement locations throughout the cleanroom. We expect vertically placed surfaces to exhibit a significantly lower CL [13]. Perhaps alarmingly, the vertically placed sample and the sample with only one week of exposure are not noticeably cleaner than the others. One explanation is that all samples were exposed to a similar amount of contamination during the handling process, and these results are not representative of the SQZ chamber environment. Future work will help elucidate this matter.

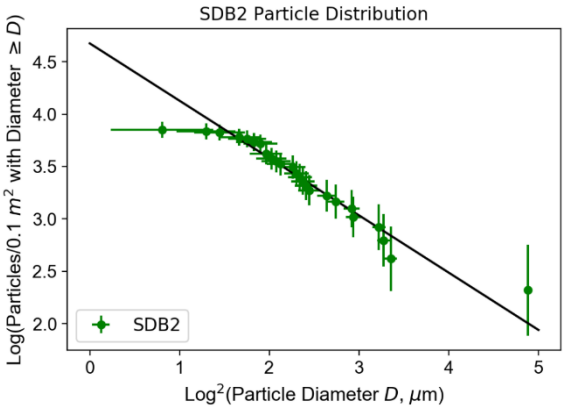

FIG 6: Number of particles on the SDB2 floor with diameter $\geq D$ (N_p) versus D on a log-log^2 scale. Fitting to Eq. 2 yields $S = -0.55 \pm 0.03$ and $CL = 840 \pm 150$.

Location	S	CL
SDB2	-0.55 ± 0.03	840 ± 150
EDB	-0.55 ± 0.02	780 ± 110
Plexi	-0.46 ± 0.03	820 ± 180
SQZV (placed vertically)	-0.47 ± 0.06	700 ± 300
WS1 (1 week exposure)	-0.38 ± 0.04	1300 ± 500

FIG 7: Results of fitting particle count data from images taken with LED height 60 mm and $NA = 5.6$ to Eq. 2. Each location is described in the Appendix.

Since IEST-STD-CC1246D requires linear N_p on a log-log^2 scale, we considered two other possible models: Gaussian and uniform distributions of particles by diameter (selected because they may be used in FRED to model dust contamination). These models do provide better fits for some distributions, but they always display negative concavity, while our data occasionally displays positive concavity.

However, it may be useful to investigate the accuracy of these models or incorporate an additional degree of freedom into particle distribution models in future work.

Seemingly small fluctuations in CL or S calculated from IEST-STD-CC1246D yield significantly different representations of the environment's cleanliness. We illustrate this by using different CL and S values to calculate cleanroom class. With equations given by Spyak [12], we derived the following formula to calculate cleanroom class given arbitrary CL and S:

$$X_c = 10^{exp} \tag{3}$$

with

$$exp = \frac{1}{0.773}\left[|S|\log(CL)^2 + 1.699 - 0.489|S| - \log(\rho) - \log(t)\right] \tag{4}$$

where ρ is a constant relating to the number of air changes per hour and t is the time in days the sample was exposed. We set $\rho = 2851$ (for 15-20 air changes per hour [13]) and $t = 30$, then calculated X_c for $S = -0.926$, $S = -0.50$ (the weighted average of the slopes given in Fig. 7), $CL = 500$ (a previously calculated value that assumes $X_c = 10000$), and $CL = 800$ (the weighted average of the CL values given in Fig. 7). Results of these calculations are shown in Fig. 8. The effect of our own analysis yielding such drastically different S than the accepted value and the high error on our CL values on the calculated X_c is enormous. Clearly, ascertaining air cleanliness from surface cleanliness data requires more precision than our current data provides.

S	CL	X_c
-0.926	800	212680
-0.926	500	9076
-0.50	800	9
-0.50	500	1.6

FIG 8: Dependence of cleanliness class (X_c) on particle distribution slope (S) and surface cleanliness

5. Conclusion

We have identified a procedure for determining surface particulate contamination in a cleanroom environment and presented data on the cleanliness of the SQZ subsystem at Virgo. We found no correlation between cleanliness level (CL) and particle distribution slope (S) in data taken at LIGO. CL and S were calculated by fitting particle counts to Eq. 2, given by IEST-STD-CC1246D. These values will serve as an input for a raytracing program that will model light scattering in the SQZ subsystem. While other particle distributions available in the raytracing program may better fit some data, IEST-STD-CC1246D appears to be the best overall. Future work may investigate how to incorporate more degrees of freedom into a particle distribution model and implement that model in programs that determine light scattering. Finally, we note that calculations of air cleanliness from surface cleanliness require a much higher confidence in CL and S values than our current data provides.

6. Acknowledgements

I would like to thank Dr. Giacomo Ciani, Dr. Livia Conti, and Beatrice D'Angelo for the wealth of insight, encouragement, and support they provided over the course of this project. I would also like to thank the University of Florida Physics Department for facilitating the

program and the National Science Foundation for supporting this project through grants PHY-1460803 and PHY-1950830.

7. References

[1] Virgo Collaboration, "Advanced Virgo," Retrieved from http://public.virgo-gw.eu/advanced-virgo/ (2020).

[2] Eric Fest. Stray light analysis and control. PM229:228, 2013.

[3] IEST-STD-CC1246D: Product cleanliness levels and contamination control program, Institute of Environmental Sciences and Technology (2002).

[4] O. Hamberg and E. Shon, "Particle size distribution on surfaces in clean rooms," Aerospace Corporation report (1984).

[5] R. Peterson, P. Magallanes, and D. Rock, "Tailored particle distributions derived from MIL-STD-1246," Proc. SPIE 4774, 79–96 (2002) [doi: 10.1117/12.481665].

[6] J. Fleming, B. Matheson, M. Dittman, F. Grochocki, and B. Firth, "Modeling particle distributions for stray light analysis," Proc. SPIE 6291, 62910T (2006).

[7] G. Ciani and F. Sorrentino, "Dust contamination witness samples placed in DetLab," Virgo internal document Virgo Logbook-49008 (June 2020).

[8] F. Sorrentino, "Optical system for dust contamination monitoring via Si wafer inspection (CRQ 2017/008)," Virgo internal document VIR-0463A-17 (2017).

[9] S. Waller, "Step by Step Procedure for aLigo Particle Imaging Using Nikon D7100 and MATLAB," LIGO internal document LIGO- T1400515-v9 (2015).

[10] C. Torrie and K. Gushwa, "Summary of 4" Wafer Data," LIGO internal document LIGO-G1400142-v1 (2015).

[11] M. Heintze, "Latest results of LLO HAM wafer analysis-------yes we are winning the fight," LIGO internal document LLO-9144 (2013).

[12] P. Spyak and W. Wolfe, "Scatter from particulate-contaminated mirrors. part 4: properties of scatter from dust for visible to far-infrared wavelengths," Opt. Eng. 31(8), 1746–1756 (1992).

[13] J. D. Buch and M. K. Barsh. Analysis of Particulate Contamination Buildup On Surfaces. 0777:43 – 54, 1987.

Appendix: Location of Samples in SQZ Chambers

The placement of each sample described in this paper is detailed below. Unless otherwise specified, all samples had one month of exposure.

SDB2: on top of threshold of tower structure, behind detection bench minitower

EDB: on top of external detection bench EDB

Plexi: on the plexiglass cover over external squeezer bench ESBQ

SQZV: on external squeezer bench ESQB

WS1: on the optical bench ESBQ, 1 week exposure

All information about sample placement is given by Ciani and Sorrentino in their logbook entry [7]. Fig. 9 shows images of sample placement.

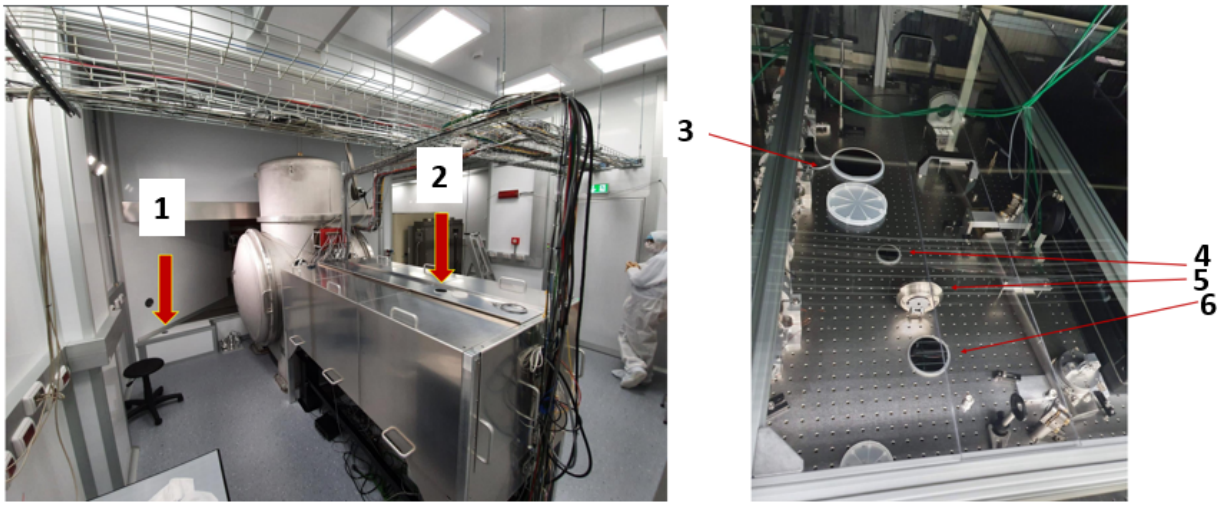

FIG 9: Placement of witness wafers labelled 1) SDB2 2) EDB 3) Plexi 4) WS2 5) SQZV 6) SQZH.